Perpendicular magnetic anisotropy induced by antiferromagnetic Fe_xMn_{1-x} alloy films: Influence of antiferromagnetic spin structure and long-range ordering

Bo-Yao Wang,* Fang-Tien Lin, Yu-Chieh Huang, Fang-Yi Li, Chi-Hsun Chen, Ke-Hong Lu, and Bo-Xiang Liao
Department of Physics, National Changhua University of Education, Changhua 500, Taiwan

(Received 5 April 2024; accepted 31 May 2024; published 11 June 2024)

Antiferromagnets show potential as materials for generating perpendicular magnetic anisotropy (PMA) in neighboring ferromagnetic (FM) thin films. In this study, we investigate the behaviors of PMA induction and the underlying mechanisms in a series of epitaxially grown face-centered-cubic-like Fe_xMn_{1-x}/Co/Fe/Cu(001) antiferromagnetic (AFM)/FM films. Our research reveals that decreasing the Fe composition ratio enhances the long-range AFM ordering of Fe_xMn_{1-x} films. When the Fe composition ratio is lower than approximately 0.3, the impact of the AFM Fe_xMn_{1-x} films on inducing PMA in the adjacent FM layer shifts from enhancement to suppression, providing important clues to a transformation in the spin structures of AFM Fe_xMn_{1-x} films from a FeMn-like three-dimensional quadratic structure to an Mn-like two-dimensional layered structure. Our findings elucidate the compositional effects of AFM Fe_xMn_{1-x} films on inducing PMA in the adjacent FM layer, as well as their relationship with the AFM spin structure and long-range AFM ordering, thereby showing the potential of $Fe_{0.4}Mn_{0.6}$ ultrathin films as promising candidates for effectively generating PMA. Such insights are crucial for understanding the AFM spin configuration of Fe_xMn_{1-x} alloy films and for furthering the control of PMA using AFM layers.

DOI: 10.1103/PhysRevB.109.214416

I. INTRODUCTION

Antiferromagnets play a pivotal role in modern spintronic devices due to their capacity to modulate the magnetic properties of neighboring ferromagnets through interfacial exchange coupling. The induced coupling effects, such as coercivity enhancement, exchange bias [1–3], and even magnetic anisotropy induction [4–11], prove advantageous for stabilizing magnetization or manipulating the magnetic easy direction of layers in steady-state spintronic devices [12,13]. Furthermore, antiferromagnets have played a crucial role in facilitating the rapid dynamic control of magnetic moments using short-pulse magnetic/electric fields or lasers in the realm of antiferromagnetic spintronics [14–17]. Based on previous studies, these antiferromagnet-induced phenomena are primarily influenced by two key factors: the AFM spin structure and the long-range AFM ordering. These factors are particularly critical for achieving stable antiferromagnet-induced perpendicular magnetic anisotropy (PMA) in ferromagnetic (FM) films, which is essential for the development of state-of-the-art perpendicular-based spintronic devices [18–21], as it may necessitate antiferromagnetic (AFM) layers with both an AFM spin structure containing an out-of-plane uncompensated component and a sufficiently high AFM ordering temperature [22,23].

FeMn alloy films are one of the candidates for the design of modern spintronic devices composed of spin-valve or spin Hall effects [24–26]. Recent investigations [22,23] have indicated that face-centered-cubic (fcc)-$Fe_{0.5}Mn_{0.5}$ can induce PMA in adjacent FM films at room temperature through collinear-like coupling, attributed to the presence of an uncompensated spin component at the [001] surface in a three-dimensional quadratic ($3Q$)-type spin structure of $Fe_{0.5}Mn_{0.5}$ [27–30]. However, the Néel temperature (T_N) of bulk FeMn is approximately 500 K [28,31], which is much lower than the values of those antiferromagnets utilized in practical spintronic devices, such as IrMn alloy (T_N ranging from 730 K to 1000 K) [32,33], MnPt ($T_N \approx 970$ K) [34,35], and NiMn ($T_N \approx 1070$ K) [36–38]. Therefore, research on enhancing the AFM ordering temperature of FeMn films while preserving the AFM spin characteristics for the PMA induction is crucial for realizing the practical application of antiferromagnet-induced PMA. Given the significant influence of alloy composition on the magnetization, long-range magnetic order, and magnetic anisotropy of various FM systems in previous studies [39–43], this work employs a variation of elemental composition as a method to alter the long-range AFM ordering and AFM spin structure of FeMn films. Notably, the behavior of antiferromagnet-induced PMA in adjacent FM films is anticipated to be highly sensitive to the AFM spin structure of the AFM film [22,23]. Therefore, a comprehensive examination of FeMn/FM films with diverse alloy compositions of FeMn could not only expand the potential applications for PMA control but also provide valuable insights into the spin structures of FeMn alloy systems, which are essential for theoretical calculations due to the lack of experimental consensus on the spin configuration in FeMn alloys with different compositions [27,31,44,45].

In this paper, we present a comprehensive investigation into the crystalline structure and the phenomenon of PMA induction in a series of epitaxially grown

*Contact author: bywang1735@cc.ncue.edu.tw

Fe_xMn_{1-x}/Co/Fe/Cu(001) films. These films vary in thickness from 0 to 10 monolayers (ML) of Fe_xMn_{1-x}, with a fixed thickness of 3 ML for Co and 3 ML for Fe, and encompass alloy composition ratio x ranging from 0 to 0.77 [46,47]. Our research reveals that a decrease in the Fe composition ratio leads to an enhancement in the long-range AFM ordering of Fe_xMn_{1-x} films. However, when Fe composition ratio is lower than approximately 0.3, the impact of the AFM Fe_xMn_{1-x} films on inducing PMA in the adjacent FM layer shifts from enhancement to suppression, suggesting a transformation in the spin structures of AFM Fe_xMn_{1-x} films from a FeMn-like $3Q$ structure to an Mn-like two-dimensional layered structure. Our discoveries clarify the compositional impacts of AFM Fe_xMn_{1-x} films on PMA induction in the neighboring FM layer, thereby demonstrating that ultrathin $Fe_{0.4}Mn_{0.6}$ films are promising candidates for the efficient control of PMA of adjacent FM films. These insights play a pivotal role in comprehending the AFM spin configuration of Fe_xMn_{1-x} alloy films and advancing the control of PMA with AFM layers.

II. EXPERIMENT

In this work, the growth conditions, crystalline structure, and magnetic properties of a series of 0–10 ML Fe_xMn_{1-x}/3-ML Co/3-ML Fe/Cu(001) films were investigated *in situ* within a multifunctional ultrahigh vacuum chamber with a base pressure of 2×10^{-10} torr. Cu(001) single-crystal substrates with miscut angles less than 0.1° underwent cycles of 2-keV Ar^+ ion sputtering and annealing at 800 K for 5 min to achieve a well-ordered crystalline structure and a smooth surface. All the films were deposited onto Cu(001) at room temperature using electron beam evaporators. Three electron beam evaporators were utilized to deposit the Fe, Co, and Mn elements, employing rod-shaped sources for Fe and Co and Mo crucible filling for Mn. The deposition rate and film thickness during growth were monitored using medium-energy electron diffraction (MEED). Figure 1 displays typical specular MEED (0,0) beam intensities for Fe films grown on Cu(001), Co films grown on 3-ML Fe/Cu(001), and various Fe_xMn_{1-x} alloy films grown on 3-ML Co/3-ML Fe/Cu(001) (Co/Fe/Cu). All MEED curves of these films reveal regular oscillations, indicating a layer-by-layer growth condition. For Fe_xMn_{1-x} grown on Co/Fe/Cu, it is notable that relatively clear oscillations appear when Fe composition ratio is between 0.39 and 0.64, indicating that these Fe_xMn_{1-x} alloy films exhibit a better layer-by-layer growth condition than others; this result is consistent with prior research on Fe_xMn_{1-x}/Co/Cu(001) [48,49].

The in-plane and vertical interlayer distances of the Fe_xMn_{1-x} alloy films were determined using low-energy electron diffraction (LEED) with a kinematic approximation (LEED I/V), as reported in reference [50]. The magnetic hysteresis loops of the films were measured *in-situ* using the longitudinal and polar magneto-optical Kerr effect (MOKE) with a He-Ne laser at room temperature. The magnetic field was aligned parallel to the film surface in the longitudinal mode and perpendicular in the polar mode. Both longitudinal and polar MOKE utilized a 45° angle between the laser beam and the sample, with measurement signals obtained using a photo-modulator and lock-in technique.

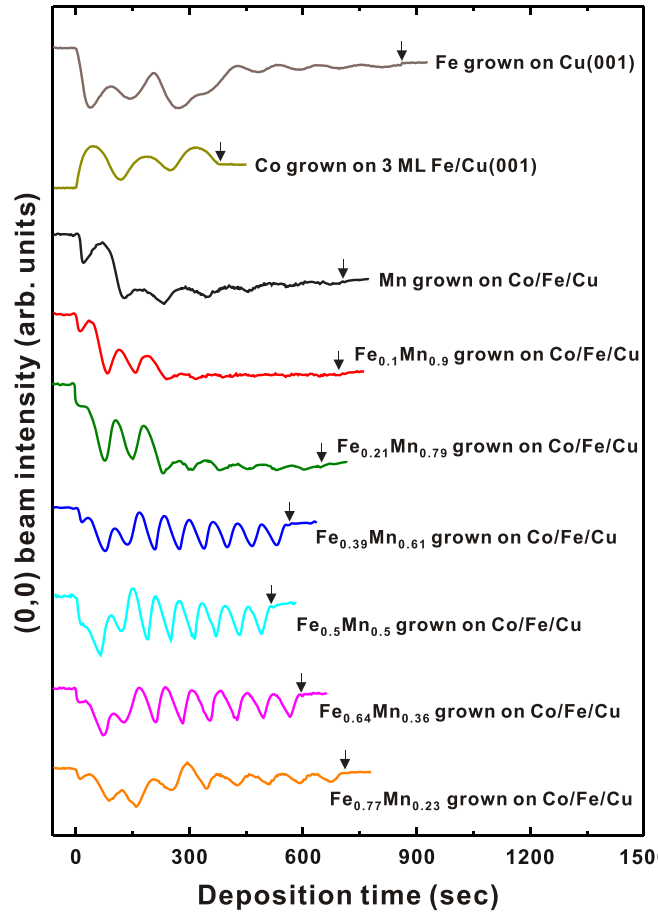

FIG. 1. Selected MEED (0,0) beam intensity curves as a function of deposition time for the Fe film grown on Cu(001), Co film grown on 3-ML Fe/Cu(001), and a series of Fe_xMn_{1-x} films grown on 3-ML Co/3-ML Fe/Cu(001) (Co/Fe/Cu) at 300 K. The film thickness was determined from the oscillations in the MEED curves. The arrows indicate the moment the shutter was closed.

III. RESULTS

A. Crystalline structure of Fe_xMn_{1-x} films grown on Co/Fe/Cu

Figures 2(a) to 2(i) show selected LEED patterns of Cu(001) substrate, Co/Fe/Cu, 10-ML Fe_xMn_{1-x}/Co/Fe/Cu with a variation of x from 0 to 0.77, respectively. These LEED patterns were measured at 110 eV in 300 K. We found that the p(1×1) spots of the grown 10-ML Fe_xMn_{1-x} films are in the same positions as those of Co/Fe/Cu and Cu(001), indicating the epitaxial growth condition of these films. Thus, the in-plane lattice constants ($a_\parallel$) of 10-ML Fe_xMn_{1-x} films with x varying from 0 to 0.77, and Co/Fe/Cu film were found to be 3.61 Å [the lattice constant of Cu(001)]. No additional ordered LEED spots were observed for Fe_xMn_{1-x} films with x from 0 to 0.77 films grown on Co/Fe/Cu, suggesting that these Fe_xMn_{1-x} films are chemically disordered crystalline films. This result is similar to the behaviors of Fe_xMn_{1-x} grown on Co [48].

Figure 3(a) illustrates the average interlayer distance ($d_\perp$) values for 0–10-ML Fe_xMn_{1-x}/Co/Fe/Cu films, with x values of 0, 0.1, and 0.21, calculated from the LEED I/V curves similar to Fig. 3(d). In Mn/Co/Fe/Cu films, $d_\perp$ value

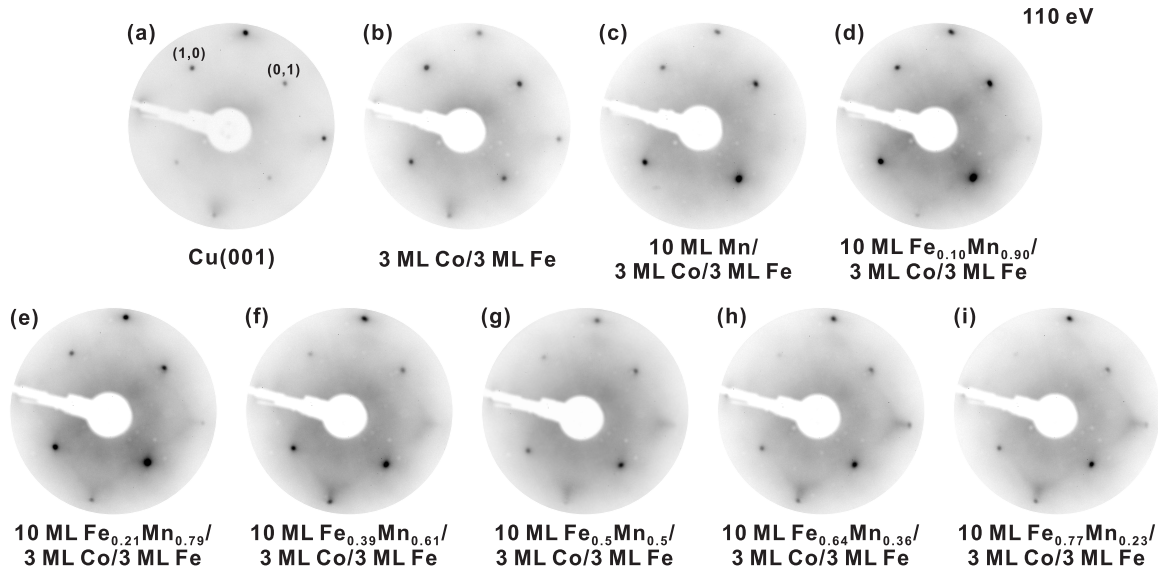

FIG. 2. Selected LEED patterns of (a) Cu(001), (b) 3 ML Co/3-ML Fe/Cu(001) (Co/Fe/Cu), (c–i) 10 ML Fe_xMn_{1-x}/Co/Fe/Cu with $x = 0$, 0.1, 0.21, 0.39, 0.5, 0.64, and 0.77, measured at 110 eV and 300 K.

stabilizes around 1.89 Å when the Mn film thickness (t_{Mn}) reaches approximately 6 ML. This indicates a formation of vertical expanded face-centered tetragonal (e-fct) structure ($c/a \approx 1.04$) of Mn film, which is consistent with a prior report [23]. A similar variation trend of $d_\perp$ with increasing FeMn thickness (t_{FeMn}) was also observed in Fe_xMn_{1-x}/Co/Fe/Cu films with x equal to 0.1 and 0.21. However, upon t_{FeMn} reaching 6 ML, the $d_\perp$ values of these Fe_xMn_{1-x} alloy films stabilize at lower values, approximately 1.86 Å–1.84 Å. Figure 3(b) further illustrates the $d_\perp$ values of 0–10-ML Fe_xMn_{1-x}/Co/Fe/Cu films with x values ranging from 0.39 to 0.77. For x values ranging from 0.39 to 0.64, the $d_\perp$ values of the Fe_xMn_{1-x} films stabilize around 1.81 Å, indicating the formation of an fcc structure. When x is increased to 0.77, the $d_\perp$ value of $Fe_{0.77}Mn_{0.23}$/Co/Fe/Cu films decreases slightly to 1.79 Å. These findings align with previous observation results in Fe_xMn_{1-x} films grown on Cu(100) [51] or bulk Fe_xMn_{1-x} [31]. Figure 3(c) presents a summary of the evolution of $d_\perp$ in 10-ML Fe_xMn_{1-x}/Co/Fe/Cu films with x ranging from 0 to 0.77. For $x \leqslant 0.21$, Fe_xMn_{1-x} films exhibit a Mn-like $d_\perp$ value of 1.89 Å, while for $0.39 \leqslant x \leqslant 0.64$, they display a $Fe_{0.5}Mn_{0.5}$-like $d_\perp$ of 1.81 Å. According to the LEED results depicted in Fig. 2, the in-plane lattice distances of 10-ML Fe_xMn_{1-x} films grown on Co/Fe/Cu, with x ranging from 0 to 0.77, are identical. Hence, the structural variation from e-fct to fcc-like in these Fe_xMn_{1-x} films could mainly be attributed to a decrease in $d_\perp$.

B. Magnetic properties of Fe_xMn_{1-x}/Co/Fe/Cu

Figure 4(a) illustrates the magnetic hysteresis loops of the 0–10 ML Mn/Co/Fe/Cu measured at 300 K. In-plane magnetic anisotropy was observed in the Co/Fe/Cu film. When t_{Mn} exceeds 4 ML, weak perpendicular magnetization was observed in Mn/Co/Fe/Cu. As detailed in prior reports [23,52], the observed weak perpendicular magnetization in Mn/Co/Fe/Cu systems is attributed to the establishment of noncollinear coupling between the interfacial Mn/Co moments, facilitated by interface crystalline anisotropy [52–54], and the AFM moments of the Mn films. However, this weak perpendicular magnetization diminishes further as t_{Mn} increases to 8 and 10 ML, attributed to a competition between the enhanced in-plane exchange coupling from the in-plane oriented spin moments of the thicker AFM Mn films and the existing perpendicular interface crystalline anisotropy of the interfacial Mn/Co moments [55,56]. Similar behavior of induced weak PMA, but with relatively higher perpendicular magnetization values compared to Mn/Co/Fe/Cu films, was observed in $Fe_{0.1}Mn_{0.9}$/Co/Fe/Cu and $Fe_{0.21}Mn_{0.79}$/Co/Fe/Cu films as t_{FeMn} reaches 6 ML [Figs. 4(b) and 4(c)]. In both cases, the induced perpendicular magnetization increases slightly as t_{FeMn} increases to approximately 8 ML but decreases when t_{FeMn} reaches 10 ML. As x in Fe_xMn_{1-x}/Co/Fe/Cu is up to 0.39 and 0.5 [Figs. 4(d) and 4(e)], much stronger PMA can be induced when t_{FeMn} reaches approximately 7 and 8 ML, respectively. However, in contrast to the cases with x ranging from 0 to 0.21 [Figs. 4(a) to 4(c)], the strength of the induced PMA in $Fe_{0.39}Mn_{0.61}$/Co/Fe/Cu and $Fe_{0.5}Mn_{0.5}$/Co/Fe/Cu monotonically increases with an increase in t_{FeMn} from 8 to 10 ML. As x reaches 0.77, no PMA can be induced in Fe_xMn_{1-x}/Co/Fe/Cu with t_{FeMn} up to 10 ML, as shown in Fig. 4(f).

To understand the relationship between the induced PMA in Fe_xMn_{1-x}/Co/Fe/Cu and the antiferromagnetism of the Fe_xMn_{1-x} films, it was crucial to identify the initiation of long-range AFM ordering within the Fe_xMn_{1-x} films. Previous studies [57–61] utilized x-ray magnetic linear dichroism (XMLD) as a direct method for examining the long-range AFM order in AFM films. However, obtaining distinguishable XMLD spectra for the current metallic AFM Fe_xMn_{1-x} films with varying alloy composition was challenging due to the low XMLD signal resulting from small Mn concentration and weak multiplet effect of these metallic films [3]. Therefore, in this study, we characterized the onset of long-range AFM

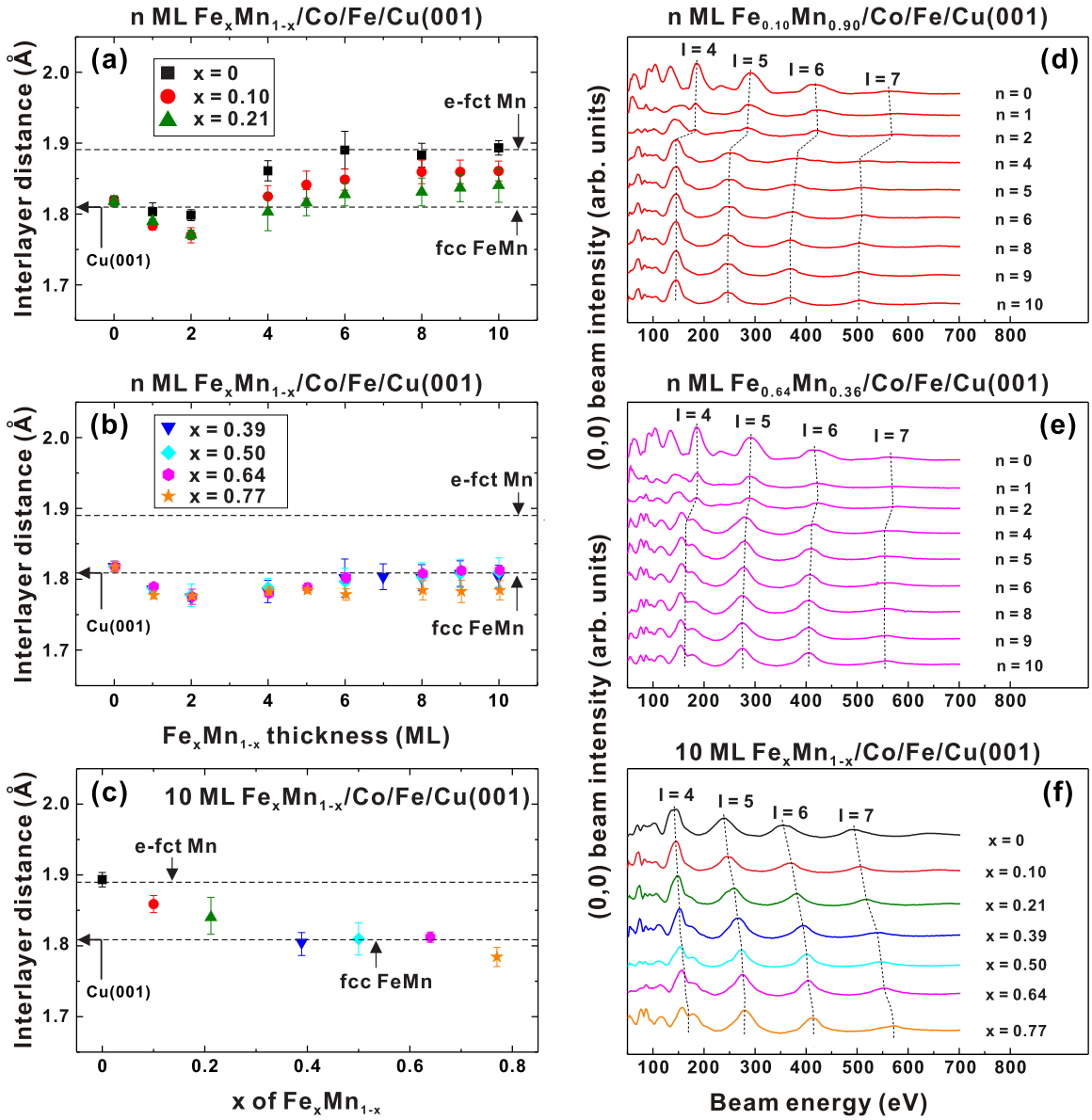

FIG. 3. The average interlayer distance ($d_\perp$) of various Fe_xMn_{1-x} films grown on Co/Fe/Cu with (a) x = 0, 0.1, 0.21, and (b) x = 0.39, 0.5, 0.64, 0.77, as calculated according to the energy peaks (I) of the corresponding LEED specular spot I/V curves of (d) and (e), respectively, measured at 300 K. (c) $d_\perp$ of various 10-ML Fe_xMn_{1-x} grown on Co/Fe/Cu calculated according to LEED I/V curves of (f), respectively, measured at 300 K.

ordering in the Fe_xMn_{1-x} films by observing the fingerprint-like phenomenon of increased coercivity value (H_c) in the coupled AFM/FM systems, which is induced by AFM-induced exchange coupling (see detailed explanation in Sec. S2 of the Supplemental Material [64]). This approach has been justified in numerous previous studies on AFM/FM thin film systems [1,5,48,62,63].

Figures 5(a) to 5(d) present the summarized in-plane and perpendicular remanent magnetization (M_r) values of 0–10 ML Fe_xMn_{1-x}/Co/Fe/Cu, with x ranging from 0.1 to 0.5, extracted from hysteresis loops similar to those in Fig. 4. Corresponding H_c values are shown in Figs. 5(e) to 5(h), respectively. In the case of $Fe_{0.1}Mn_{0.9}$/Co/Fe/Cu [Fig. 5(a)], a weak perpendicular magnetization was observed when t_{FeMn} exceeds a threshold value of approximately 4 ML, indicated by the blue shadow. Additionally, an increase in the H_c value was also observed in $Fe_{0.1}Mn_{0.9}$/Co/Fe/Cu when t_{FeMn} exceeds 4 ML [Fig. 5(e)], indicating the establishment of long-range AFM ordering of the $Fe_{0.1}Mn_{0.9}$ film at this threshold, as depicted by a green shadow and t_{FeMn}^{AFM}. Thus, the discovery of similar threshold values of t_{FeMn} for these two behaviors suggests that the establishment of long-range AFM ordering of the $Fe_{0.1}Mn_{0.9}$ film could be the underlying cause of the induced weak perpendicular magnetization in $Fe_{0.1}Mn_{0.9}$/Co/Fe/Cu. In Fe_xMn_{1-x}/Co/Fe/Cu systems with x ranging from 0.21 to 0.5, we observed also a consistent threshold of t_{FeMn} that leads to an enhancement of H_c [Figs. 5(f) to 5(h)] and the development of either weak or strong PMA [Figs. 5(b) to 5(d)]. These findings reaffirm that the induced PMA in Fe_xMn_{1-x}/Co/Fe/Cu could be triggered

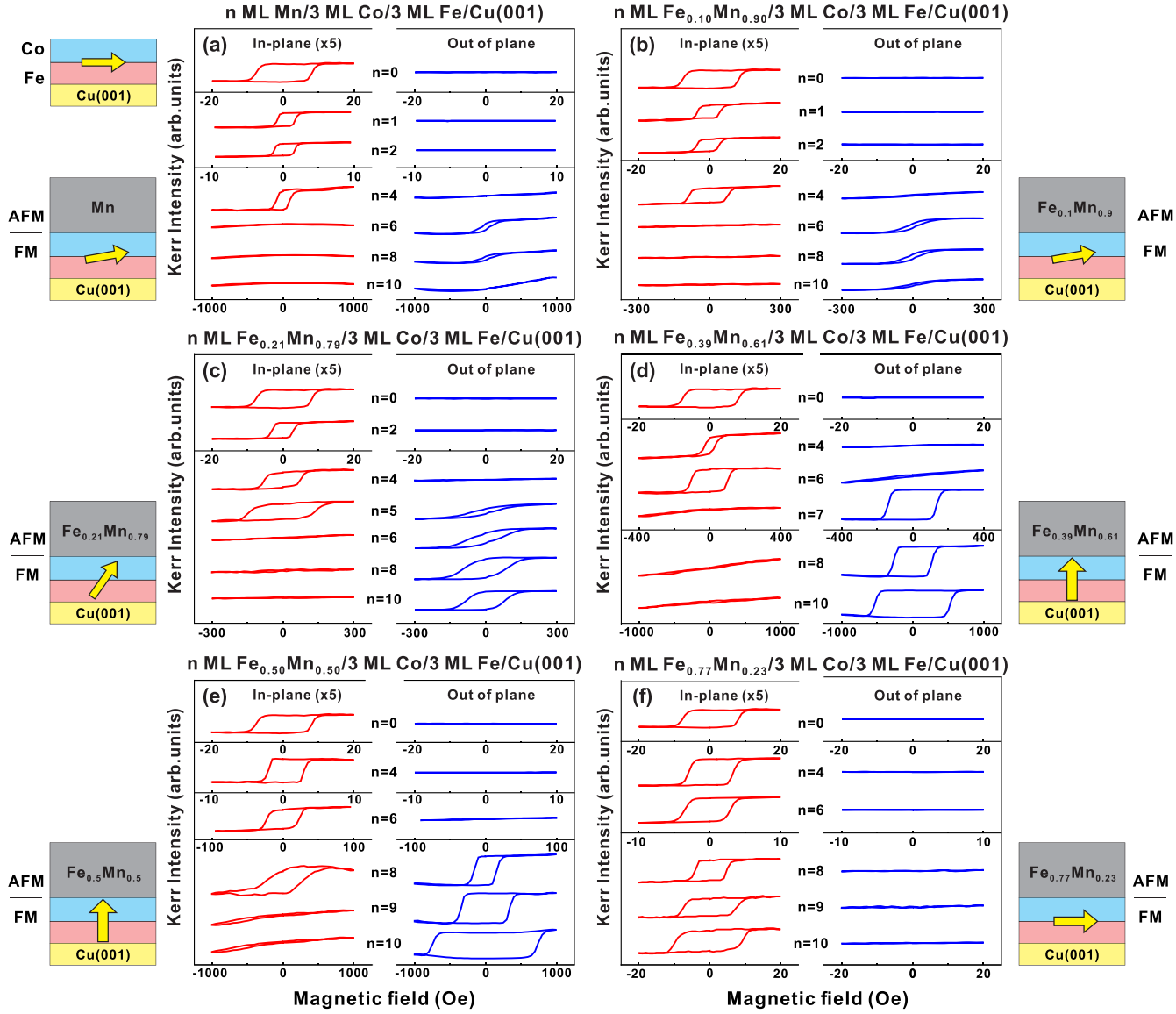

FIG. 4. Magnetic hysteresis loops of 0–10 ML Fe_xMn_{1-x}/Co/Fe/Cu with (a) x = 0, (b) x = 0.1, (c) x = 0.21, (d) x = 0.39, (e) x = 0.5, (f) x = 0.77, measured using longitudinal and polar MOKE at 300 K.

by AFM Fe_xMn_{1-x} films through AFM–FM exchange coupling.

Figure 6(a) summarizes a magnetic easy axis phase diagram of 0–10-ML Fe_xMn_{1-x}/Co/Fe/Cu with x ranging from 0 to 0.77, as given by Fig. 4 and Fig. S1(a) of the Supplemental Material [64]. As x ranging 0 to 0.21, a transition from an in-plane to a weak perpendicular magnetic state occurs when t_{FeMn} reaches 4–6 ML, corresponding to the threshold of t_{FeMn} for an establishment of long-range AFM ordering, t_{FeMn}^{AFM}, as indicated by the green dashed line. However, within the same x range of 0 to 0.21, the strength of the induced weak PMA in Fe_xMn_{1-x}/Co/Fe/Cu tends to decrease as t_{FeMn} increased further. On the other hand, for x ranging from 0.39 to 0.64, strong PMA of Fe_xMn_{1-x}/Co/Fe/Cu can be triggered when t_{FeMn} reaches t_{FeMn}^{AFM} (7–9 ML). However, PMA is further enhanced with an increase in t_{FeMn} to 10 ML. These findings clearly distinguish different characteristic behaviors of induced magnetic anisotropy in adjacent Co/Fe/Cu films by AFM Fe_xMn_{1-x} films when x values fall within different regimes.

IV. DISCUSSION

A. PMA induction by Fe_xMn_{1-x} alloy films: Roles of long-range AFM ordering and AFM spin structure

Based on the preceding results, it becomes evident that the PMA induction behaviors in Fe_xMn_{1-x}/Co/Fe/Cu films exhibit high sensitivity to the t_{FeMn} and alloy composition of Fe_xMn_{1-x} films, wherein both the AFM long-range ordering and AFM spin configuration are likely significant contributing factors. To elucidate the impact of these factors, we further investigated the evolution of the induced PMA strength in 10 ML Fe_xMn_{1-x}/Co/Fe/Cu films with varying x values. This analysis is conducted based on the magnetic hysteresis loops in Fig. 4 and Fig. S1(b) of the Supplemental Material [64].

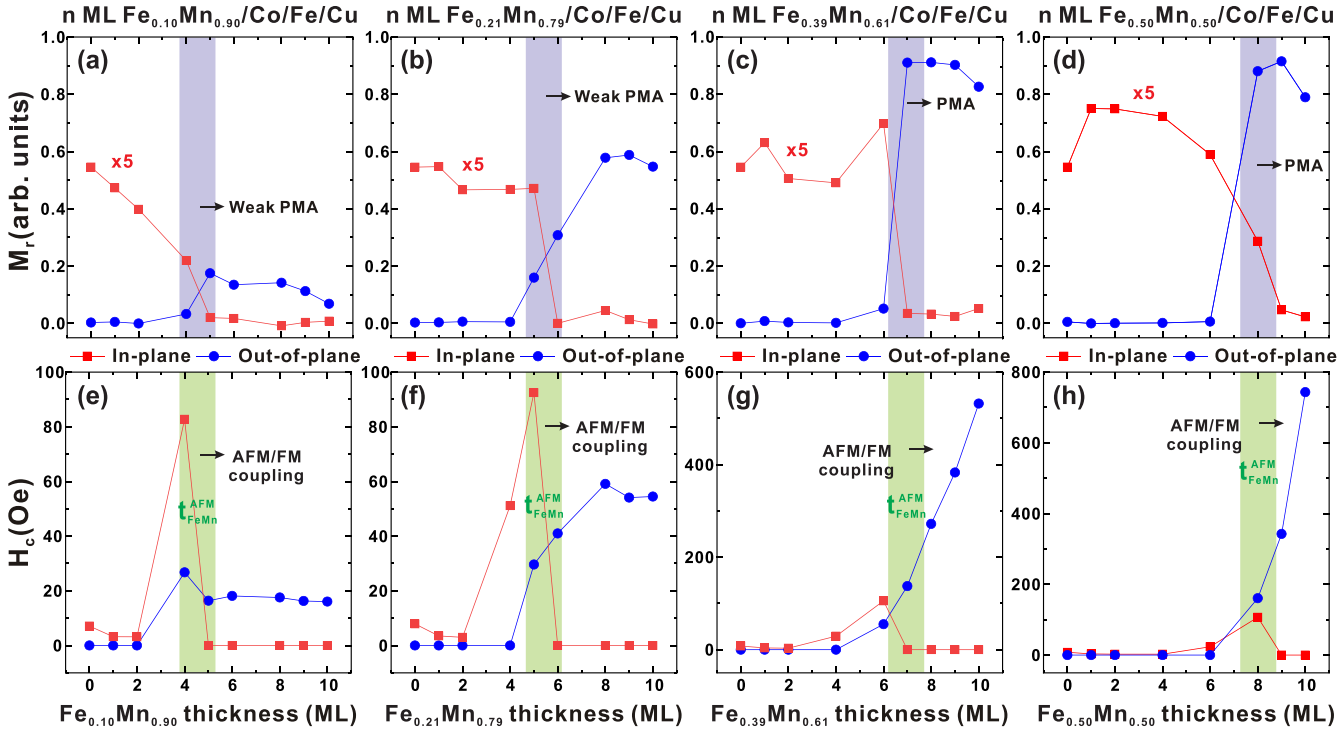

FIG. 5. The summarized values of (a–d) M_r and (e–h) H_c for 0–10 ML Fe_xMn_{1-x}/Co/Fe/Cu with $x = 0.1, 0.21, 0.39, 0.5$, extracted from the magnetic hysteresis loops depicted in Fig. 4. The shaded regions highlight a similar threshold thickness of t_{FeMn} for the onset of induced PMA (blue color) and Fe_xMn_{1-x}-induced AFM-FM exchange coupling (green color; t^{AFM}_{FeMn}) in Fe_xMn_{1-x}/Co/Fe/Cu.

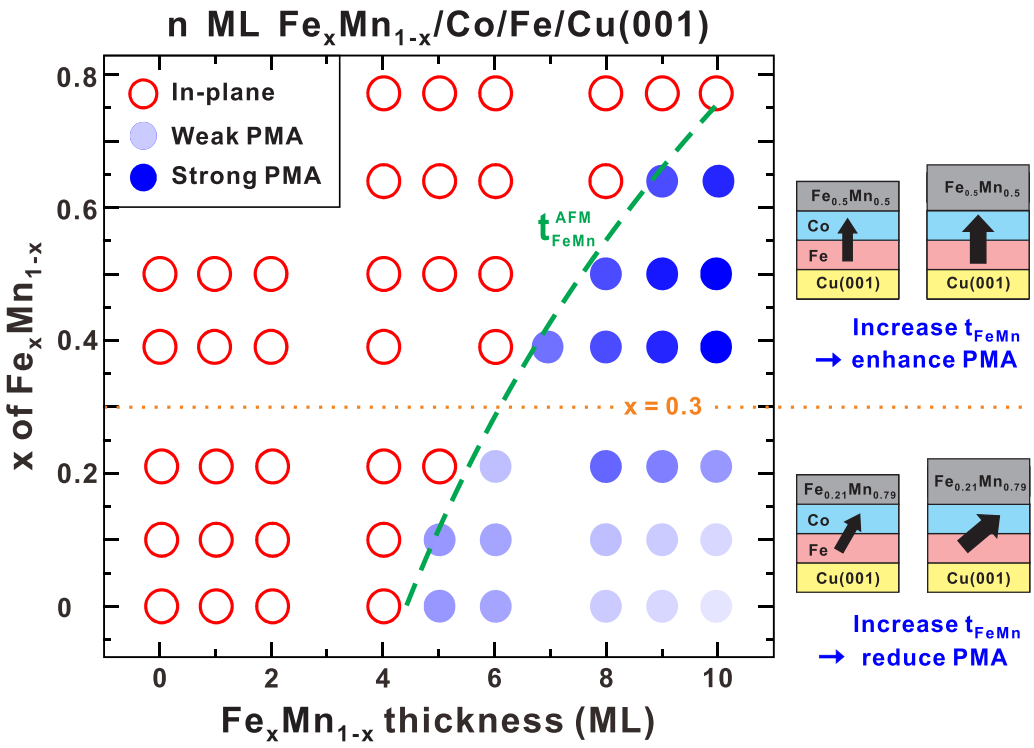

FIG. 6. Magnetic easy axis phase diagrams of 0–10 ML Fe_xMn_{1-x}/Co/Fe/Cu plotted as a function of x and t_{FeMn} at 300 K, based on longitudinal and polar MOKE measurements. Red open circles (light to dark blue solid circles) indicate the presence of in-plane (weak to strong perpendicular) magnetic anisotropy of the films. The dashed green line depicts the estimated boundary of t^{AFM}_{FeMn}, as shown in Figs. 5(e)–5(h), marking the onset of AFM-FM exchange coupling and long-range AFM ordering of Fe_xMn_{1-x} films. The illustrations in the right of the figure indicate that AFM Fe_xMn_{1-x} films, with x values lower and higher than approximately 0.3, respectively, can lead to suppression and enhancement of induced PMA in adjacent Co/Fe/Cu films.

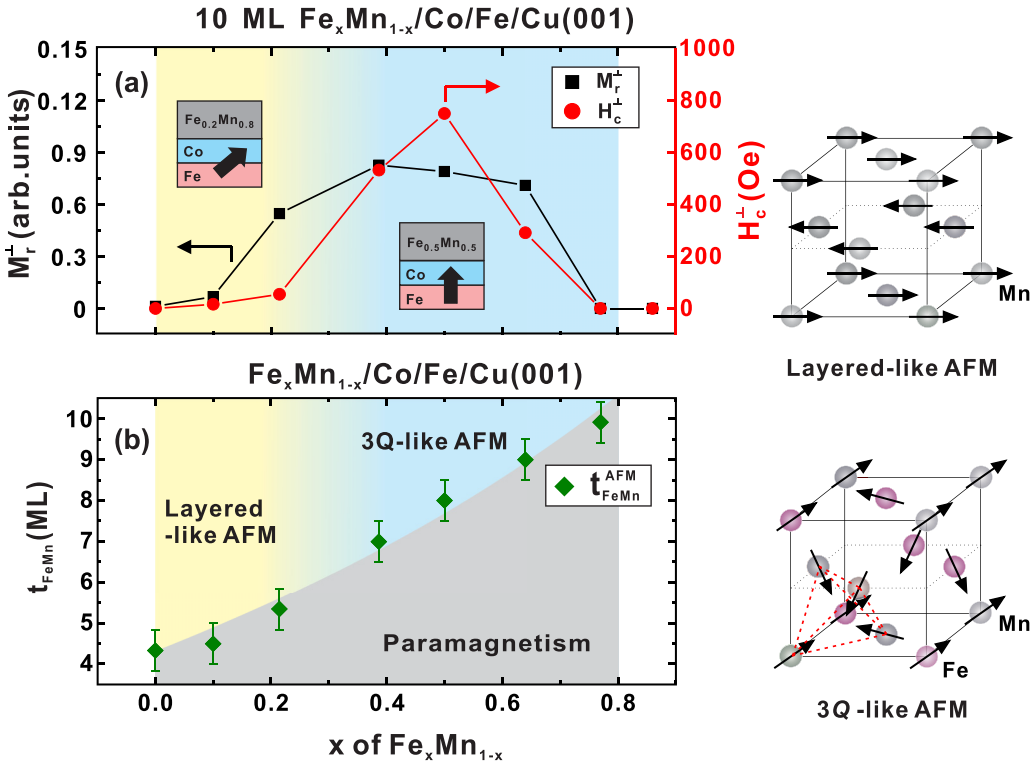

FIG. 7. (a) The summarized values of M_r (left-axis) and H_c (right-axis) of 10-ML Fe_xMn_{1-x}/Co/Fe/Cu films with varying x extracted from magnetic hysteresis loops similar to those shown in Fig. 4 and Fig. S1(a) of the Supplemental Material [64]. (b) The threshold thicknesses t_{FeMn}^{AFM} marking the onset of AFM-FM exchange coupling and the establishment of long-range AFM ordering in Fe_xMn_{1-x} films. The yellow and blue regions denote coupling behaviors potentially induced by AFM Fe_xMn_{1-x} films that could have in-plane layered [55,56] and 3Q-like structures [29,31], as illustrated on the right side of the figure, respectively.

In Fig. 7(a), the perpendicular M_r value exhibits an increasing trend with x, reaching a peak as x approaches 0.39 and then maintaining a consistently high level within the range $x = 0.39$–0.64. Subsequently, the perpendicular M_r value declines as x reaches 0.77. Meanwhile, the perpendicular H_c value experiences rapid growth after $x > 0.3$, peaking around $x \approx 0.5$ and declining further with increasing x. Given the higher M_r and H_c values depicted in Fig. 7(a), along with square perpendicular magnetic hysteresis loops [Figs. 4(d) and 4(e)], we concluded a total alignment of perpendicular magnetization in 10-ML Fe_xMn_{1-x}/Co/Fe/Cu films within the range $x = 0.39$–0.64. Additionally, the Stoner-Wohlfarth model [65] has suggested that a magnetic system with giant uniaxial anisotropy, such as PMA, will be accompanied by an increase in H_c along the easy magnetic direction, where the anisotropy constant K_u is proportional to both H_c and magnetization values [10]. Therefore, 10-ML $Fe_{0.5}Mn_{0.5}$/Co/Fe/Cu film, with a presence of maximum values concurrently for perpendicular M_r and H_c, exhibits the strongest induced PMA compared to other systems.

Next, we examined the relationship between PMA induction strength in 10 ML Fe_xMn_{1-x}/Co/Fe/Cu films and the long-range AFM ordering of 10-ML Fe_xMn_{1-x} films, with a variation of x. Figure 7(b) displays the threshold values t_{FeMn}^{AFM}, for triggering H_c enhancement in Fe_xMn_{1-x}/Co/Fe/Cu films in room temperature, as analyzed from Fig. 5 and Fig. S2 of Supplemental Material [64]. As mentioned, t_{FeMn}^{AFM} values indicate the onset of long-range AFM ordering in Fe_xMn_{1-x} films [1,5,48,62]. Noting that the values of t_{FeMn}^{AFM} monotonically increase with the increase of x, this suggests that at a fixed t_{FeMn}, the long-range AFM ordering of Fe_xMn_{1-x} decreases as x increases. Given that the long-range AFM ordering of 10-ML $Fe_{0.5}Mn_{0.5}$ is weaker than that of Fe_xMn_{1-x} alloy films with $x < 0.5$, the observed higher strength of induced PMA in 10-ML $Fe_{0.5}Mn_{0.5}$/Co/Fe/Cu films, compared to systems with lower x values, cannot be attributed to the impact of long-range AFM ordering. Therefore, the AFM spin structure of $Fe_{0.5}Mn_{0.5}$ film must be the more crucial contributing factor.

In previous studies, Kuch *et al*. provided experimental evidence for a three-dimensional noncollinear AFM spin structure in ultrathin single-crystalline fcc $Fe_{0.5}Mn_{0.5}$ layers through x-ray magnetic circular (linear) dichroism measurements [29]. Their findings align with the proposed 3Q spin structure in bulk $Fe_{0.5}Mn_{0.5}$ [31]. Our current investigation observed that the AFM $Fe_{0.5}Mn_{0.5}$ layer can induce strong PMA on adjacent Co/Fe/Cu layers. The induced PMA can also be effectively explained by the existence of out-of-plane uncompensated magnetic moments in a 3Q noncollinear spin structure of AFM $Fe_{0.5}Mn_{0.5}$ film; these moments initiate collinear-like coupling with the moments of adjacent FM films [22,23]. On the other hand, Hsu *et al*. and Wu *et al*. have identified a layered AFM spin structure for Mn films grown on Co/Cu(001) layers through spin-polarized scanning tunneling microscopy (SP-STM) measurements [55,56]. However, previous studies have indicated that thin Mn films deposited on

Co/Fe(Ni) layers typically enhance the perpendicular interface crystalline anisotropy of the Mn/Co interfacial moments due to interface electronic hybridization [52–54]. When t_{FeMn} is close to $t_{\mathrm{FeMn}}^{\mathrm{AFM}}$, the interplay between the interfacial Mn/Co moments and the AFM moments of the Mn films leads to the establishment of noncollinear coupling at the AFM-FM interface, resulting in the presence of weak perpendicular magnetization in Mn/Co/Fe/Cu films [23,52]. As t_{Mn} of the AFM Mn film increases further, the enhanced in-plane exchange coupling from the in-plane oriented spin moments of the thicker AFM Mn films [55,56] could compete with the existing perpendicular interface crystalline anisotropy of the Mn/Co interfacial moments. This competition could potentially either maintain or reduce the strength of the induced weak PMA in adjacent FM films, thereby presenting a nontrivial behavior of PMA induction strength with an increase in t_{Mn}, as depicted in Fig. 4(a) [23,52].

Given a high correlation between the proposed AFM spin structures of $Fe_{0.5}Mn_{0.5}$ (or Mn) layers and characteristic behaviors of induced magnetic properties on adjacent Co/Fe/Cu film, our research findings could provide important clues for comprehending the AFM spin structure of Fe_xMn_{1-x} films with other alloy compositions. According to Figs. 5 and 7, Fe_xMn_{1-x} films with $x < 0.3$ exhibit characteristic behaviors of inducing nontrivial PMA strength with an increase in t_{FeMn} on Co/Fe/Cu, similar to the behavior caused by Mn films. Therefore, the spin structure of these Fe_xMn_{1-x} films may resemble the layered AFM structure of the Mn film [55,56]. When x exceeds approximately 0.3, the influence of the AFM Fe_xMn_{1-x} films on inducing PMA in the adjacent FM layer shifts from suppression to enhancement, suggesting a transformation in the spin structures of AFM Fe_xMn_{1-x} films. Because the characteristic PMA-induction behaviors induced by Fe_xMn_{1-x} films are pretty similar as x varies from 0.39 to 0.64, the AFM spin structure of the Fe_xMn_{1-x} alloy in this range may resemble the $3Q$-like noncollinear spin structure [22,23]. Indeed, the composition range of the $3Q$ spin structure in Fe_xMn_{1-x} estimated in this work aligns with the boundaries of x, which range approximately from 0.35 to 0.80, as proposed previously in bulk Fe_xMn_{1-x} derived from Mössbauer and neutron diffraction experiments [31]. Moreover, as illustrated in Fig. 7, our experiments show that the change in PMA induction behavior in 10-ML Fe_xMn_{1-x}/Co/Fe/Cu is gradual when x varies from 0.64 to 0.21. This finding suggests that the AFM spin structure of Fe_xMn_{1-x} films may not transition sharply within this range of x values. According to prior reports, T_N of bulk $Fe_{0.5}Mn_{0.5}$ is approximately 500 K [28,31]. In our current study, based on the results presented in Fig. 7(b), a relatively higher T_N in $Fe_{0.5}Mn_{0.5}$ films can be achieved by increasing the Mn concentration. Considering the need for higher induced PMA strength [Fig. 7(a)] and a thinner AFM Fe_xMn_{1-x} layer ($t_{\mathrm{FeMn}}^{\mathrm{AFM}}$) [Fig. 7(b)], at room temperature, $x = 0.4$ could be identified as the optimal condition for ultrathin AFM Fe_xMn_{1-x} films to induce stable PMA on the adjacent FM layer.

Previous research has indicated that the magnetic states of Fe_xMn_{1-x} alloys are not only sensitive to the alloy composition but also highly correlated with the crystalline structure [30,66]. A transition from antiferromagnetism to ferromagnetism could even be induced by structural phase transitions in highly strained-fcc or -body-centered-cubic $Fe_{0.5}Mn_{0.5}$ epitaxial films [66]. In this study, by observing the induced magnetic behaviors, we provide experimental insights into the spin structure of AFM Fe_xMn_{1-x} alloy films, whose ground state configuration remains ambiguous. Furthermore, we detail their crystalline structure, providing a more experimental basis for theoretical research on Fe_xMn_{1-x} alloys with varying compositions.

B. Effects of local interface condition changes on AFM-FM coupling and PMA induction

In addition to the previously mentioned effects of uniform Fe_xMn_{1-x} films, we further discussed the impact of local interfacial FeMn alloying on AFM-FM coupling and PMA induction. As shown in Figs. 4(a)–4(c), Mn-rich Fe_xMn_{1-x} (with x ranging from 0 to 0.21) induces only weak perpendicular magnetization on the adjacent Co/Fe/Cu layer. However, recent research has found that doping 50% Fe at the Mn/Co interface can induce a much stronger PMA on the adjacent Co/Fe/Cu layer [23]. This finding demonstrates that, without causing significant changes in the overall lattice structure, the variations in the spin structure of the interface and local exchange coupling significantly influence the behavior of PMA induction. In addition, Ref. [67] shows that embedding a 2–3 ML thin $Fe_{0.5}Mn_{0.5}$ layer between Mn and Co/Fe/Cu films strengthens the PMA of the Co/Fe/Cu layer. This enhancement occurs because these $Fe_{0.5}Mn_{0.5}$ spacer layers can achieve an AFM state due to the magnetic proximity effects of the upper Mn layer. Conversely, if the Mn layer is embedded between the $Fe_{0.5}Mn_{0.5}$ and Co/Fe/Cu films, the strength of PMA induction is weakened due to the exchange anisotropy induced by the in-plane oriented AFM structure of the Mn films. These recent research reports have indicated that, besides the influence of the entire AFM films, the local AFM spin structure and exchange coupling at the AFM-FM interface are also crucial for inducing PMA in these AFM/FM systems. This finding aligns with the effects of Mn interface doping in exchange bias coupling systems [68].

Additionally, according to the current results, variations in the FeMn alloy composition lead to changes in $d_\perp$ (Fig. 3), which may influence the interfacial Mn moments or the $3d$-$3d$ exchange interaction. These factors could also affect the PMA induction behavior of the adjacent Co/Fe/Cu film. Indeed, a previous study reported that for fcc-like Mn films, a decrease in $d_\perp$ significantly weakens the PMA induction effect [53]. This is attributed to the enhanced interlayer coupling between Mn layers with an in-plane oriented layered AFM spin structure [55,56]. In the present work, Mn-rich Fe_xMn_{1-x}/Co/Fe/Cu films (with x ranging from 0 to 0.21) show that $d_\perp$ decreases with increased Fe concentration [Figs. 3(a) and 3(c)]. However, the strength of the induced PMA is clearly enhanced [Figs. 5(a) and 5(b)]. As inferred from the results of previous work [53], the promotion of PMA induction by these Mn-rich Fe_xMn_{1-x} films with increasing x is unlikely to be attributed to the effects of a slight reduction in $d_\perp$. Instead, a deviation in the local AFM structure from the "pure" in-plane layered AFM structure could be a dominant factor. On the other hand, Fe_xMn_{1-x} films with x ranging from 0.39 to 0.64 reveal a relatively stable $d_\perp$

value [Figs. 3(b) and 3(c)]. Therefore, within this x range, the variation in the strength of PMA [Figs. 5(c) and 5(d)] could be solely determined by changes in the AFM-FM exchange coupling, mediated by slight variations in the $3Q$-like AFM spin structure or moment value due to different alloy concentrations.

V. CONCLUSION

We have conducted a comprehensive investigation on the behavior of PMA induction in a series of fcc-like Fe_xMn_{1-x}/Co/Fe/Cu, where the t_{FeMn} ranges from 0 to 10 ML and the x values vary from 0 to 0.77. Our findings reveal that a decrease in the Fe composition ratio enhances the long-range AFM ordering of Fe_xMn_{1-x} films. Furthermore, when the Fe composition ratio is lower than approximately 0.3, the impact of the AFM Fe_xMn_{1-x} films on inducing PMA in the adjacent FM layer shifts from enhancement to suppression, providing essential clues to transformation in the spin structures of AFM Fe_xMn_{1-x} films from a FeMn-like $3Q$ structure to an Mn-like two-dimensional layered structure. Our discoveries clarify the compositional impacts of AFM Fe_xMn_{1-x} films on PMA induction in the neighboring FM layer, along with their correlation with the AFM spin structure and long-range AFM ordering, thereby demonstrating that ultrathin $Fe_{0.4}Mn_{0.6}$ films are promising candidates for the efficient control of PMA of adjacent FM films. These insights are invaluable for comprehending the AFM spin configuration of Fe_xMn_{1-x} and advancing the control of PMA with AFM layers.

ACKNOWLEDGMENTS

This work was partly supported by the National Science and Technology Council, Taiwan (Grant No. NSTC 112-2112-M-018-006).

[1] J. Nogués and I. K. Schuller, Exchange bias, J. Magn. Magn. Mater. **192**, 203 (1999).
[2] S. D. Bader, Opportunities in nanomagnetism, Rev. Mod. Phys. **78**, 1 (2006).
[3] J. Stöhr and H. C. Siegmann, Magnetism: *From Fundamentals to Nanoscale Dynamics* (Springer, New York, NY, 2006).
[4] W. Kuch, F. Offi, L. I. Chelaru, M. Kotsugi, K. Fukumoto, and J. Kirschner, Magnetic interface coupling in single-crystalline Co/FeMn bilayers, Phys. Rev. B **65**, 140408(R) (2002).
[5] C. Won, Y. Z. Wu, H. W. Zhao, A. Scholl, A. Doran, W. Kim, T. L. Owens, X. F. Jin, and Z. Q. Qiu, Studies of FeMn/Co/Cu(001) films using photoemission electron microscopy and surface magneto-optic Kerr effect, Phys. Rev. B **71**, 024406 (2005).
[6] Q. F. Zhan and K. M. Krishnan, In-plane reorientation of magnetization in epitaxial exchange biased Fe/MnPd bilayers, Appl. Phys. Lett. **96**, 112506 (2010).
[7] P. Kuświk, P. L. Gastelois, M. M. Soares, H. C. N. Tolentino, M. De Santis, A. Y. Ramos, A. D. Lamirand, M. Przybylski, and J. Kirschner, Effect of CoO/Ni orthogonal exchange coupling on perpendicular anisotropy of Ni films on Pd(001), Phys. Rev. B **91**, 134413 (2015).
[8] P. Kuświk, B. Szymański, B. Anastaziak, M. Matczak, M. Urbaniak, A. Ehresmann, and F. Stobiecki, Enhancement of perpendicular magnetic anisotropy of Co layer in exchange-biased Au/Co/NiO/Au polycrystalline system, J. Appl. Phys. **119**, 215307 (2016).
[9] B. Y. Wang, N. Y. Jih, W. C. Lin, C. H. Chuang, P. J. Hsu, C. W. Peng, Y. C. Yeh, Y. L. Chan, D. H. Wei, W. C. Chiang, and M. T. Lin, Driving magnetization perpendicular by antiferromagnetic-ferromagnetic exchange coupling, Phys. Rev. B **83**, 104417 (2011).
[10] B.-Y. Wang, J.-Y. Hong, K.-H. O. Yang, Y.-L. Chan, D.-H. Wei, H.-J. Lin, and M.-T. Lin, How antiferromagnetism drives the magnetization of a ferromagnetic thin film to align out of plane, Phys. Rev. Lett. **110**, 117203 (2013).
[11] H. Omura, S. Komori, S. Arai, K. Yoda, K. Imura, and T. Taniyama, Controllable perpendicular magnetic anisotropy in $Fe/Fe_{100-x}Rh_x$ heterostructures probed by ferromagnetic resonance, Phys. Rev. Appl. **19**, 064077 (2023).
[12] S. Mao, Z. Gao, H. Xi, P. Kolbo, M. Plumer, L. Wang, A. Goyal, I. Jin, J. Chen, C. Hou, R. M. White, and E. Murdock, Spin-valve heads with self-stabilized free layer by antiferromagnet, IEEE Trans. Magn. **38**, 26 (2002).
[13] R. K. Han, L. Liu, H. L. Sun, H. R. Qin, X. P. Zhao, D. Pan, D. H. Wei, and J. H. Zhao, Large tunable perpendicular magnetic anisotropy in ultrathin co-based ferromagnetic films induced by antiferromagnetic δ-Mn, Phys. Rev. Appl. **19**, 024033 (2023).
[14] T. Jungwirth, X. Marti, P. Wadley, and J. Wunderlich, Antiferromagnetic spintronics, Nat. Nanotechnol. **11**, 231 (2016).
[15] N. Thielemann-Kühn, D. Schick, N. Pontius, C. Trabant, R. Mitzner, K. Holldack, H. Zabel, A. Föhlisch, and C. Schüßler-Langeheine, Ultrafast and energy-efficient quenching of spin order: Antiferromagnetism beats ferromagnetism, Phys. Rev. Lett. **119**, 197202 (2017).
[16] I. Kumberg, E. Golias, N. Pontius, R. Hosseinifar, K. Frischmuth, I. Gelen, T. Shinwari, S. Thakur, C. Schüßler-Langeheine, P. M. Oppeneer, and W. Kuch, Accelerating the laser-induced demagnetization of a ferromagnetic film by antiferromagnetic order in an adjacent layer, Phys. Rev. B **102**, 214418 (2020).
[17] E. Golias, I. Kumberg, I. Gelen, S. Thakur, J. Gördes, R. Hosseinifar, Q. Guillet, J. K. Dewhurst, S. Sharma, C. Schüßler-Langeheine, N. Pontius, and W. Kuch, Ultrafast optically induced ferromagnetic state in an elemental antiferromagnet, Phys. Rev. Lett. **126**, 107202 (2021).
[18] S. Mangin, D. Ravelosona, J. A. Katine, M. J. Carey, B. D. Terris, and E. E. Fullerton, Current-induced magnetization reversal in nanopillars with perpendicular anisotropy, Nat. Mater. **5**, 210 (2006).
[19] Y. Shiroishi, K. Fukuda, I. Tagawa, H. Iwasaki, S. Takenoiri, H. Tanaka, H. Mutoh, and N. Yoshikawa, Future options for HDD storage, IEEE Trans. Magn. **45**, 3816 (2009).
[20] S. Ikeda, K. Miura, H. Yamamoto, K. Mizunuma, H. D. Gan, M. Endo, S. Kanai, J. Hayakawa, F. Matsukura, and H. Ohno,

A perpendicular-anisotropy CoFeB-MgO magnetic tunnel junction, Nat. Mater. **9**, 721 (2010).

[21] D. C. Worledge, G. Hu, D. W. Abraham, J. Z. Sun, P. L. Trouilloud, J. Nowak, S. Brown, M. C. Gaidis, E. J. O'Sullivan, and R. P. Robertazzi, Spin torque switching of perpendicular Ta|CoFeB|MgO-based magnetic tunnel junctions, Appl. Phys. Lett. **98**, 022501 (2011).

[22] B.-Y. Wang, M.-S. Tsai, C.-W. Huang, C.-W. Shih, C.-J. Chen, K. Lin, J.-J. Li, N.-Y. Jih, Chun-I Lu, T.-H. Chuang, and D.-H. Wei, Effects of the antiferromagnetic spin structure on antiferromagnetically induced perpendicular magnetic anisotropy, Phys. Rev. B **96**, 094416 (2017).

[23] B.-Y. Wang, J.-Y. Ning, T.-H. Li, C.-C. Chung, C.-Y. Hsu, M.-S. Tsai, T.-H. Chuang, and D.-H. Wei, Effects of the antiferromagnetic spin structure on antiferromagnetically induced perpendicular magnetic anisotropy, Phys. Rev. B **105**, 184415 (2022).

[24] G. W. Anderson, Y. Huai, and M. Pakala, Spin-valve thermal stability: The effect of different antiferromagnets, J. Appl. Phys. **87**, 5726 (2000).

[25] W. Zhang, M. B. Jungfleisch, W. Jiang, J. E. Pearson, A. Hoffmann, F. Freimuth, and Y. Mokrousov, Spin hall effects in metallic antiferromagnets, Phys. Rev. Lett. **113**, 196602 (2014).

[26] X. Li, X. Liu, H. Li, Y.-Q. Lü, and C. Gao, Ultrathin copper films grown on SrTiO3 substrates for epitaxy of single-crystalline γ-FeMn, J. Appl. Phys. **134**, 063902 (2023).

[27] J. S. Kouvel and J. S. Kasper, Long-range antiferromagnetism in disordered Fe-Ni-Mn alloys, J. Phys. Chem. Solids **24**, 529 (1963).

[28] H. Umebayashi and Y. Ishikawa, Antiferromagnetism of γ Fe-Mn Alloys, J. Phys. Soc. Jpn. **21**, 1281 (1966).

[29] W. Kuch, L. I. Chelaru, F. Offi, J. Wang, M. Kotsugi, and J. Kirschner, Three-dimensional noncollinear antiferromagnetic order in single-crystalline FeMn ultrathin films, Phys. Rev. Lett. **92**, 017201 (2004).

[30] M. Ekholm and I. A. Abrikosov, Structural and magnetic ground-state properties of γ-FeMn alloys from ab initio calculations, Phys. Rev. B **84**, 104423 (2011).

[31] Y. Endoh and Y. Ishikawa, Antiferromagnetism of γ iron manganes alloys, J. Phys. Soc. Jpn. **30**, 1614 (1971).

[32] T. Yamaoka, Antiferromagnetism in γ-phase Mn-Ir alloys, J. Phys. Soc. Jpn. **36**, 445 (1974).

[33] K. O'Grady, L. E. Fernandez-Outon, and G. Vallejo-Fernandez, A new paradigm for exchange bias in polycrystalline thin films, J. Magn. Magn. Mater. **322**, 883 (2010).

[34] E. Krén, G. Kádár, L. Pál, J. Sólyom, P. Szabó, and T. Tarnóczi, Magnetic structures and exchange interactions in the Mn-Pt system, Phys. Rev. **171**, 574 (1968).

[35] R. Y. Umetsu, K. Fukamichi, and A. Sakuma, Electrical and magnetic properties, and electronic structures of pseudo-gap-type antiferromagnetic L10-type MnPt alloys, Mater. Trans. **47**, 2 (2006).

[36] M. F. Toney, M. G. Samant, T. Lin, and D. Mauri, Thickness dependence of exchange bias and structure in MnPt and MnNi spin valves, Appl. Phys. Lett. **81**, 4565 (2002).

[37] P. M. Oppeneer, H.-C. Mertins, D. Abramsohn, A. Gaupp, W. Gudat, J. Kuneš, and C. M. Schneider, Buried antiferromagnetic films investigated by x-ray magneto-optical reflection spectroscopy, Phys. Rev. B **67**, 052401 (2003).

[38] J. S. Kasper and J. S. Kouvel, The antiferromagnetic structure of NiMn, J. Phys. Chem. Solids **11**, 231 (1959).

[39] A. Dittschar, W. Kuch, M. Zharnikov, and C. M. Schneider, Interrelation of morphology, structure, and magnetism in Fe_xCo_{1-x}/Cu(100) epitaxial alloy films, J. Magn. Magn. Mater. **212**, 307 (2000).

[40] T. Burkert, L. Nordström, O. Eriksson, and O. Heinonen, Giant magnetic anisotropy in tetragonal FeCo alloys, Phys. Rev. Lett. **93**, 027203 (2004).

[41] F. Yildiz, F. Luo, C. Tieg, R. M. Abrudan, X. L. Fu, A. Winkelmann, M. Przybylski, and J. Kirschner, Strongly enhanced orbital moment by reduced lattice symmetry and varying composition of $Fe_{1-x}Co_x$ Alloy Films, Phys. Rev. Lett. **100**, 037205 (2008).

[42] M.-T. Lin, W. C. Lin, C. C. Kuo, and C. L. Chiu, Critical evolution of spin-reorientation transition in magnetic Co_xNi_{1-x}/Cu(100) films upon precise variation of *d*-band filling, Phys. Rev. B **62**, 14268 (2000).

[43] W. C. Lin, B. Y. Wang, Y. W. Liao, K.-J. Song, and M.-T. Lin, Alloying and strain relaxation effects on spin-reorientation transitions in $Co_xNi_{1-x}/Cu_3Au(100)$ ultrathin films, Phys. Rev. B **71**, 184413 (2005).

[44] S. J. Kennedy and T. J. Hick, Mössbauer investigations of a magnetic structure of γ-Fe-Mn, J. Phys. F: Met. Phys. **17**, 1599 (1987).

[45] P. Bisanti, G. Mazzone, and F. Sacchetti, Electronic structure of FCC Fe-Mn alloys. II. Spin-density measurements, J. Phys. F: Met. Phys. **17**, 1425 (1987).

[46] 3-ML Co/3-ML Fe/Cu(001) film has been reported to be a magnetic template with high magnetic moment density and flat surface [23].

[47] R. Thamankar *et al.*'s work showed that FM or ferrimagnetic order is present in $Fe_{0.81}Mn_{0.19}$ film grown Cu(001) [49].

[48] F. Offi, W. Kuch, and J. Kirschner, Structural and magnetic properties of Fe_xMn_{1-x} thin films on Cu(001) and on Co/Cu(001), Phys. Rev. B **66**, 064419 (2002).

[49] R. Thamankar, S. Bhagwat, and F. O. Schumann, Structural and magnetic properties of ultrathin fcc Fe_xMn_{1-x} films on Cu(100), Phys. Rev. B **69**, 054411 (2004).

[50] W. C. Lin, C. C. Kuo, C. L. Chiu, and M. T. Lin, Growth, crystalline structure and magnetic properties of ultrathin alloy films Co_xNi_{1-x}/Cu(100), Surf. Sci. **478**, 9 (2001).

[51] W. Pan, W.-C. Lin, N.-Y. Jih, C.-H. Chuang, Y.-C. Chen, Ch.-C. Kuo, P.-C. Huang, and M.-T. Lin, Structural phase diagram, magnetism, and exchange-biased behavior of Fe films on Fe_xMn_{1-x}/Cu(001), Phys. Rev. B **74**, 224430 (2006).

[52] B.-Y. Wang, J.-Y. Lee, W.-L. Li, K. Lin, M.-S. Tsai, T.-H. Chuang, and D.-H. Wei, Perpendicular magnetic anisotropy induced by antiferromagnetic Mn-Pd alloy films: Dual effects of exchange and spin-orbit coupling, Phys. Rev. B **107**, 104429 (2023).

[53] B.-Y. Wang, P.-H. Lin, M.-S. Tsai, C.-W. Shih, M.-J. Lee, C.-W. Huang, N.-Y. Jih, P.-Y. Cheng, and D.-H. Wei, Crucial role of interlayer distance for antiferromagnet-induced perpendicular magnetic anisotropy, Phys. Rev. B **92**, 214435 (2015).

[54] B.-Y. Wang, C.-H. Hsiao, B.-X. Liao, C.-Y. Hsu, T.-H. Li, Y.-L. Hsu, Y.-M. Lai, M.-S. Tsai, T.-H. Chuang, and D.-H. Wei, Perpendicular magnetic anisotropy induced by NiMn-based antiferromagnetic films with in-plane spin orientations: Roles of

interfacial and volume antiferromagnetic moments, Phys. Rev. B **104**, 024424 (2021).

[55] P.-J. Hsu, Chun-I Lu, Y.-H. Chu, B.-Y. Wang, C.-B. Wu, L.-J. Chen, S.-S. Wong, and M.-T. Lin, Layered antiferromagnetic spin structures of expanded face-centered-tetragonal Mn(001) as an origin of exchange bias coupling to the magnetic Co layer, Phys. Rev. B **85**, 174434 (2012).

[56] C. B. Wu, J. Song, and W. Kuch, Spin-polarized scanning tunneling microscopy study of Mn/Co/Cu(001) using a bulk Fe ring probe, Appl. Phys. Lett. **101**, 012404 (2012).

[57] A. Scholl, J. Stöhr, J. Lüning, J. W. Seo, J. Fompeyrine, H. Siegwart, J. P. Locquet, F. Nolting, S. Anders, E. E. Fullerton, M. R. Scheinfein, and H. A. Padmore, Observation of antiferromagnetic domains in epitaxial thin films, Science **287**, 1014 (2000).

[58] F. Nolting, A. Scholl, J. Stöhr, J. W. Seo, J. Fompeyrine, H. Siegwart, J. P. Locquet, S. Anders, J. Lüning, E. E. Fullerton, M. F. Toney, M. R. Scheinfein, and H. A. Padmore, Direct observation of the alignment of ferromagnetic spins by antiferromagnetic spins, Nature (London) **405**, 767 (2000).

[59] H. Ohldag, A. Scholl, F. Nolting, S. Anders, F. U. Hillebrecht, and J. Stöhr, Spin reorientation at the antiferromagnetic NiO(001) surface in response to an adjacent ferromagnet, Phys. Rev. Lett. **86**, 2878 (2001).

[60] W. Kim, E. Jin, J. Wu, J. Park, E. Arenholz, A. Scholl, C. Hwang, and Z. Q. Qiu, Effect of NiO spin orientation on the magnetic anisotropy of the Fe film in epitaxially grown Fe/NiO/Ag(001) and Fe/NiO/MgO(001), Phys. Rev. B **81**, 174416 (2010).

[61] W. J. Antel, Jr., F. Perjeru, and G. R. Harp, Spin structure at the interface of exchange biased FeMn/Co bilayers, Phys. Rev. Lett. **83**, 1439 (1999).

[62] K. Lenz, S. Zander, and W. Kuch, Magnetic proximity effects in antiferromagnet/ferromagnet bilayers: The impact on the Néel temperature, Phys. Rev. Lett. **98**, 237201 (2007).

[63] W. H. Meiklejohn and C. P. Bean, New magnetic anisotropy, Phys. Rev. **102**, 1413 (1956).

[64] See Supplemental Material at http://link.aps.org/supplemental/10.1103/PhysRevB.109.214416 for information on the magnetic properties of 0–10 ML Fe_xMn_{1-x}/Co/Fe/Cu(001) films with $x = 0, 0.64$, and 0.77, and a detailed explanation of the correlation between H_c enhancement and the onset of long-range AFM ordering of Fe_xMn_{1-x} films.

[65] E. C. Stoner and E. P. Wohlfarth, A mechanism of magnetic hysteresis in heterogeneous alloys, Philos. Trans. R. Soc. London A **240**, 599 (1948).

[66] Y. Hwang, S. Choi, J. Choi, and S. Cho, Induced high-temperature ferromagnetism by structural phase transitions in strained antiferromagnetic γ-$Fe_{50}Mn_{50}$ epitaxial films, Sci. Rep. **9**, 3669 (2019).

[67] B.-Y. Wang, T.-H. Li, B.-X. Liao, C.-H. Hsiao, L.-H. Chang, M.-S. Tsai, T.-H. Chuang, and D.-H. Wei, Magnetic proximity effects in antiferromagnetic composite thin films: Roles of triggering perpendicular magnetic anisotropy, Phys. Rev. B **108**, 184412 (2023).

[68] R. Carpenter, N. C. Cramp, and K. O'Grady, Effect of Mn interface doping in polycrystalline exchange bias thin films, IEEE Trans. Magn. **48**, 4351 (2012).